Carbon 155 (2019) 734–739

Contents lists available at ScienceDirect

Carbon

journal homepage: www.elsevier.com/locate/carbon

Single-walled carbon nanotube membranes for optical applications in the extreme ultraviolet range

V.M. Gubarev [a], V.Y. Yakovlev [b], M.G. Sertsu [c], O.F. Yakushev [d], V.M. Krivtsun [e, a, h], Yu.G. Gladush [b], I.A. Ostanin [a, g], A. Sokolov [c], F. Schäfers [c], V.V. Medvedev [e, a, *], A.G. Nasibulin [b, f]

[a] Center for Computational and Data-Intensive Science and Engineering, Skolkovo Institute of Sciense and Technology, Moscow, Russia
[b] Skolkovo Institute of Science and Technology, Nobel str. 3, Moscow, 121205, Russia
[c] Helmholtz Zentrum Berlin (BESSY-II), Albert-Einstein-Strasse 15, D-12489, Berlin, Germany
[d] P. N. Lebedev Physical Institute of the Russian Academy of Science, Moscow, Russia
[e] Institute of Spectroscopy of the Russian Academy of Science, Moscow, Troitsk, Russia
[f] Aalto University, 15100, FI-00076, Aalto, Finland
[g] Multi-Scale Mechanics (MSM), Faculty of Engineering Technology, MESA+, University of Twente, Enschede, The Netherlands
[h] Faculty of Physics, Higher School of Economics, Old Basmannya 21/4, Moscow, Russia

ARTICLE INFO

Article history:
Received 23 May 2019
Received in revised form
4 August 2019
Accepted 2 September 2019
Available online 5 September 2019

ABSTRACT

In this paper, we explore the possibility of using free-standing thin films from single-walled carbon nanotube (SWCNT) material in optics of the extreme ultraviolet (EUV) range. Test samples were fabricated using an aerosol chemical vapor deposition method. Synchrotron radiation was used to record the transmittance spectra of samples in the EUV range. The measured transmittance for a film 40 nm thick almost monotonously increases from 76% at a wavelength of 20 nm–99% at a wavelength of 1 nm. The measured stress-strain curve for the test samples shows that the SWCNT-based thin films have rather high ductility as opposite to fragile films made of conventional solid state materials. We use numerical simulations to demonstrate that the film strain occurs mainly by straightening and sliding of the nanotubes past each other without forming of strain localization responsible for fragile behavior. The combination of high radiation transmittance and unique mechanical properties makes the SWCNT-based thin films very promising for use in the EUV optics. In particular, such films can be used to protect delicate optical elements for EUV lithography from their contamination with debris particles.

1. Introduction

Carbon nanotubes based thin films attract considerable attention due to their unique properties, including high porosity and low density, high transmittance, low resistance and high thermal conductivity, chemical sensitivity and tunability between semiconducting and metallic properties [1–4]. These properties have already been actively examined and are expected to be carefully developed in various electronic and optical applications [5,6]. In particular, the outstanding properties of carbon nanotubes films make them extremely attractive for optics of the EUV range (wavelength ~ 10 nm). This spectral range is being actively explored at present through the development of efficient radiation sources and a number of promising applications [7–13]. Thin-film optics gains a tremendous importance in this spectral range due to the high natural absorption of all materials without exception - only matter layers with a thickness of ~10–100 nm have sufficient transparency. For this reason, free-standing thin films can be used to create such important optical elements as spectral filters, polarizers, and beam splitters [14–19]. Moreover, there is an urgent need to prevent contamination of modern optical elements with debris by elaborating a protective membrane known as a pellicle [20]. This application is especially important for EUV lithography – photolithography employing radiation with a wavelength of 13.5 nm [7]. In the process of lithography, a pattern on a photomask (reticle) is projected onto a wafer. Contamination of the photomask with debris particles can lead to defects in printed integrated

* Corresponding author. Institute of Spectroscopy of the Russian Academy of Science, Moscow, Troitsk, Russia.
E-mail address: Medvedev@phystech.edu (V.V. Medvedev).

https://doi.org/10.1016/j.carbon.2019.09.006
0008-6223/

circuits. In order to avoid contamination, a pellicle should be installed in front of the photomask [20]. There are strict requirements for the pellicle: it should have EUV transparency of around 90%, excellent thermal and chemical stability and high thermal conductivity to reduce heating by the absorbed light. It should also demonstrate excellent mechanical properties to withstand pressure drops and mechanical impacts from debris particles and fast moving mask stage.

In this paper, we propose and examine free-standing thin films based on single-walled carbon nanotubes (SWCNT) for use in short-wave optics and, in particular, in the pellicle fabrication. We investigate the optical properties of the films in the EUV spectral region and test their mechanical properties. Films are obtained by the method of scalable aerosol CVD synthesis, which allows film fabrication with lateral sizes of more than 10 cm and thicknesses from 10 to 100 nm. Low density and relatively low absorption cross-sections of carbon atoms at short wavelengths make it possible to achieve a high transmittance. For instance, we demonstrate a transmittance of 88% at the working wavelength of EUV lithography (13.5 nm) for a film 40 nm thick. SWCNT films have a natural difference in their microstructure from that of amorphous and polycrystalline solid films, and the concept of brittleness is not applicable to such films. We implement a biaxial stretching with a bulge test technique to measure mechanical properties and carried out high performance mesoscale modeling to demonstrate the microscale behavior of the SWCNT film during its deformation. The high transmittance of SWNT films in combination with outstanding mechanical characteristics provides a very attractive set of properties for EUV optics, e.g. as a strong protective membrane.

2. Sample fabrication

SWCNTs are synthesized in an aerosol (floating catalyst) CVD reactor described elsewhere [21,22]. Nanotubes grow on aerosol iron nanoparticles floating in the flow of CO atmosphere in a hot wall reactor and then are collected on a nitrocellulose filter at the outlet. They form a randomly oriented network (Fig. 1a) consisting of individual SWCNTs and their small bundles. Depending on the collection time it is possible to obtain films of different thickness from a few to hundreds of nanometers. SWCNT films can be easily transferred from the filter to various substrates using the dry transfer technique described by Kaskela et al. [23]. If the film thickness exceeds 10 nm it is possible to make free-standing films of a large area by transferring the SWCNTs on a support frame [2]. All the experimental studies reported below were carried out using samples with a thickness of 40-nm- produced in a lab scale reactor and attached to fused silica frames with 5 mm circular aperture. Nevertheless, the described method can be easily scaled to fabricate large-area films (e.g. A3-sized paper). For instance, Fig. 1b shows a photo of a freestanding SWCNT 40 nm thick film suspended above a rectangular aperture 10×13 cm^2 that satisfies the size requirements for the EUV protective pellicles [24].

3. Optical properties

Measurements of the short-wavelength transmittance of the samples were performed using s-polarized synchrotron radiation at the facilities of the optics beamline of the synchrotron radiation source BESSY-II [25,26]. The normal incident beam spot size entering the center of the sample was 0.72×0.50 mm^2. The angular alignments of the sample and detector goniometers were adjusted to an accuracy of $\pm$0.05 deg. A GaAsP photodetector with an active area of 4×4 mm^2 was used to receive direct transmitted rays and most of the scattered parts. The spectral purity of the incident beam from high order diffractions of the monochromator grating was maintained by an efficient high order suppression system installed in the beamline [27].

The measured transmittance spectrum is shown by the solid red line in Fig. 2. The transmittance T at a wavelength of 20 nm is 76%. It can be seen that T first increases to 98.2% with decreasing wavelength λ and then the transmittance drops at wavelengths just below $\lambda \approx 4.4$ nm, which corresponds to the K-edge of carbon. T takes its minimum value of 80.3% at $\lambda \approx 4.2$ nm and then increases again with decreasing wavelength. At the wavelength of 13.5 nm used by EUV lithography, the transmittance of the sample is 88%.

In Fig. 2, we also compare the measured transmittance spectrum for the SWCNTs with the calculated transmittance spectra of 40-nm-thick films of silicon, silicon nitride and graphite. The possibility of producing ultrathin free-standing films of these materials has been previously demonstrated [28–30].

Transmittance spectra were calculated using the following equation:

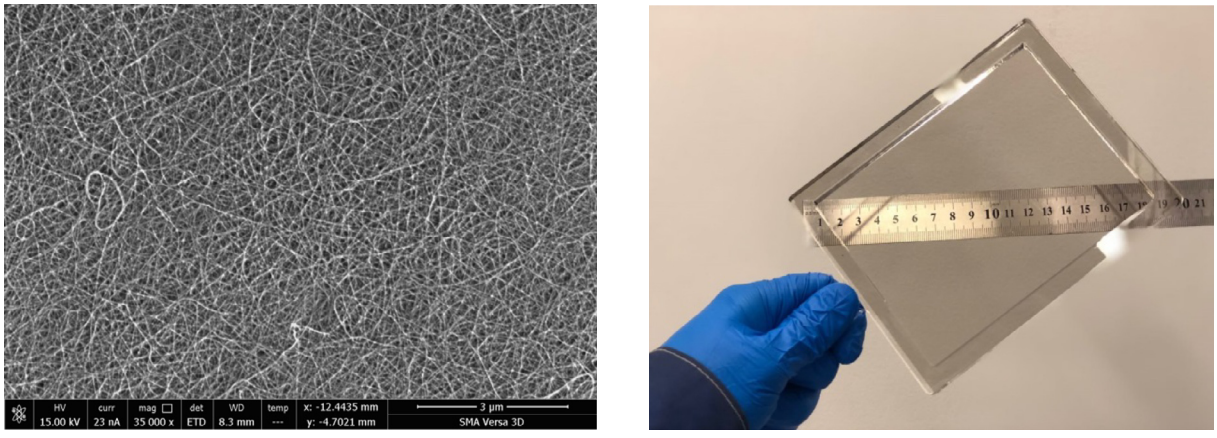

Fig. 1. a) SEM image of randomly oriented single-walled carbon nanotubes produced by an aerosol CVD synthesis. b) Photograph of a free-standing SWCNT 40 nm thick film suspended above a rectangular aperture 10×13 cm^2. (A colour version of this figure can be viewed online.)

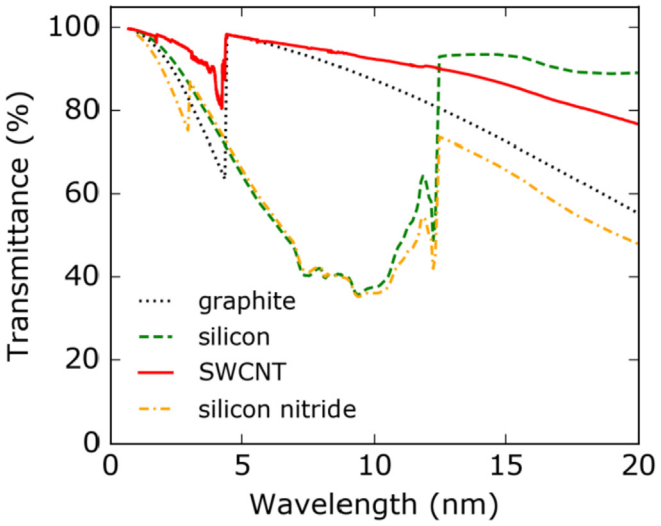

Fig. 2. Experimental transmittance spectrum for a 40-nm-thick SWCNT film (solid red line) and calculated transmittance spectra for 40-nm-thick silicon films (green dashed line), silicon nitride (or yellow dot-dashed line) and graphite (gray dotted line). (A colour version of this figure can be viewed online.)

$$T = \left| \frac{4n \exp(2\pi ind/\lambda)}{(1+n)^2 - (1-n)^2 \exp(4\pi ind/\lambda)} \right|^2, \quad (1)$$

where d denotes the film thickness, λ is the radiation wavelength, n is the complex refractive index of the material at a wavelength λ. The n values of the abovementioned materials were taken from the Henke database. It is seen that the SWCNT films promise higher transmittance than silicon nitride and graphite films in the entire considered spectral range. And SWCNT films promise a higher transmittance than pure silicon films in the range below the L–edge of the photoabsorption of Si, i.e. for $\lambda < 12.4$ nm. The higher transmittance of SWCNT films compared to graphite is due to the lower mass density of SWCNT films. We also note that the maximum possible transmittance of short-wave radiation can be achieved using membranes made of two-dimensional materials, e.g. graphene or boron nitride. For instance, a single-layer graphene sheet theoretically has a transmittance above 99% in the spectral range under consideration. However, the production of defect-free free-standing graphene sheets with a characteristic size of ~10 cm remains challenging.

4. Mechanical properties

4.1. Experimental tests

In order to evaluate mechanical properties of the studied SWCNT thin films the bulge test was used. In this test, a thin film sample is clamped over an orifice and a uniform gas pressure is applied from one of the film sides. Then the deflection of the film is measured as a function of the gas pressure which allows determining the stress-strain curve. Our experimental setup is schematically shown in Fig. 3. In the experiments we used samples of SWCNT thin films fixed on the ring-shaped fused silica substrates with a central aperture of 5 mm. The sample was hermetically clamped over the orifice dividing the vacuum chamber into two volumes V_1 and V_2 as shown in Fig. 3. These two volumes were also connected by an additional bypass to the valve. First, the entire chamber was pumped to a base pressure of 4×10^{-5} Pa. Pumping was carried out with the open bypass valve. Then, with the closed

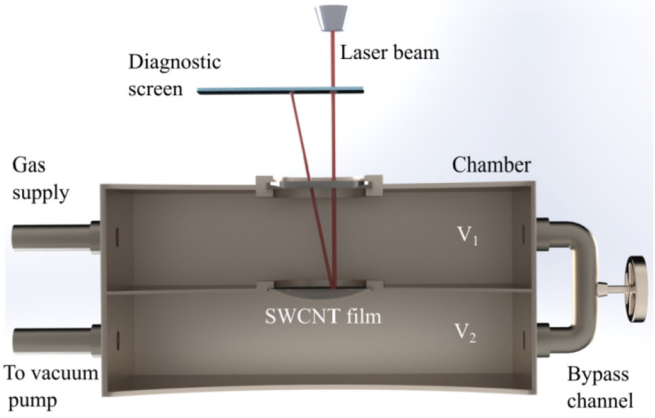

Fig. 3. Scheme of the experimental setup for the bulge test: a free standing film is deformed by gas pressure, deflecting the laser beam. Shift laser spot on the ruler gives the curvature of the film. (A colour version of this figure can be viewed online.)

bypass valve, the volume V_1 was filled with argon to a given pressure P_1, which was controlled by a manometer. Pressure in the volume V_2 denoted as P_2 was measured using an ionization gauge. Note that in the experiments the pressure difference P_2/P_1 was about 10^{-3}. The curvature of the film under pressure load was determined from the measured deflection of the reflected laser beam.

The loading pressure $\Delta P = P_1 - P_2$ causes film deformation. For small deformations, the shape of a curved film can be approximated by a sphere. As mentioned above, the radius of curvature R of the deformed film was measured by the angular deviation of the reflected laser beam. In the case of small deformations, the relative stretching of the film can be calculated by the following formula:

$$\varepsilon = \frac{2}{3}\left(\frac{h}{a}\right)^2, \quad (2)$$

where a denotes the radius of the aperture on which the film is fixed, $h \approx a^2/2R$ is the film deflection in the center. The stress σ arising in the deformed film can be calculated by the following formula:

$$\sigma = \frac{\Delta PR}{2d}, \quad (3)$$

where d denotes the film thickness. It is important to note that Eqs. (2) and (3) are derived under the assumption that in the initial state the surface of the film is flat and not stressed. In reality, it is extremely difficult to create such initial conditions. Most often, as a result of fixing on the holder, the film has non-zero initial stress, or vice versa, it becomes slack.

In these experiments, the SWCNT films were initially slack. To show that, we plot the measured film deflection h as a function of the pressure load (Fig. 4A). It is evident that h remains non-zero during the application of infinitesimal pressures, i.e. $h = h_0$ at $\Delta P = 0^+$. In this case the equation for film strain should be corrected as follows:

$$\varepsilon = \frac{2}{3a^2}\left(h^2 - h_0^2\right). \quad (4)$$

Fig. 4B shows the measured stress-strain curve for a 40-nm-thick SWCNT film. For $\varepsilon < 0.001$, the measured stress is linearly proportional to the strain. Hence, it is possible to define the biaxial modulus Y of the film in this range as $Y = \sigma/\varepsilon$. The measured data give $Y = 24.5$ GPa. For $\varepsilon > 0.001$, the linear dependence of σ on ε is

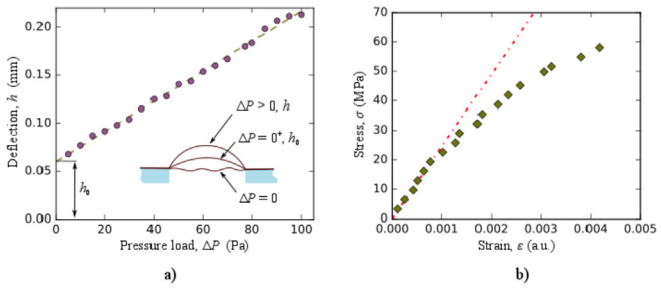

Fig. 4. A) Measured deflection of a 40-nm-thick film as a function of the load pressure in the bulge test. B) Measured stress-strain curve for a SWCNT film with a thickness of 40 nm. Red dot-dashed line corresponds to the date adjustment in the range of linear deformation with $Y = \sigma/\varepsilon = 24.5$ GPa. (A colour version of this figure can be viewed online.)

violated, but the deformation remains elastic up to the yield point of $\varepsilon = 0.003$. The measured stress at $\varepsilon = 0.003$ is $\sigma = 52$ MPa. This stress value corresponds to the experimental gas pressure load of $\Delta P \approx 80$ Pa. In the experiments, the gas pressure increased until the sample was destroyed. The corresponding pressure was as high as 5.3 kPa. At this point the deformation of the sample was so large that the probe laser beam was deflected outside the detector aperture. For this reason, it was impossible to measure the corresponding values of strain and stress. However, such a large difference in pressures corresponding to the yield and fracture points allows to conclude that the studied SWCNT films can be categorized(classified) as very ductile materials.

There is a number of publications devoted to the study of the mechanical properties of thin freestanding films made of other materials that can be used as an EUV radiation filter, e.g. SiN_x, Al and $MoSi_2$ [31,32]. These publications show that the fracture of such materials occurs on the linear part of the stress-strain curve, which characterizes such films as extremely brittle. In terms of protection of EUV optical surfaces from contamination, the ductile SWCNT films are preferable to fragile films made of conventional condensed matter materials. When destroyed under an accidental excessive mechanical load, a brittle film fixed in front of a protected optical element can contaminate the protected optical surface with fragments. In contrast, SWCNT films have a large safety margin associated with a wide range of plastic deformation.

4.2. Numerical evaluation

In order to interpret the aforementioned mechanical properties of freestanding SWCNT films, we carried out high-performance numerical simulations of the SWCNT film mechanics. For this, we used the mesoscale modeling technique [33–35]. It is based on time integration of the damped dynamics of chains of rigid cylinders, connected with 3D elastic bonds [36] and interacting via realistic coarse-grained vdW potential, which allows relative slip of SWCNTs in contact. Molecular dynamics simulation was used for the model calibration.

We tested a $2 \times 2\ \mu m^2$ SWCNT film specimen with a density of 0.35 g/cm^3, a film thickness of 20 nm, and periodic boundary conditions in the out-of-plane direction ("thick film" approximation). Two specimen sets contained 2000 (10,10) SWCNTs with a length of 0.5 μm and 1000 (10,10) SWCNTs with a length of 1 μm. At the initial stage of numerical experiments, straight SWCNTs were deposited on a plane with uniform random in-plane orientations and slight out-of-plane deviations, and then relaxed to a minimum energy state, forming a network of interconnected bundles due to the van der Waals (vdW) adhesion (Fig. 5a. The equilibration of the

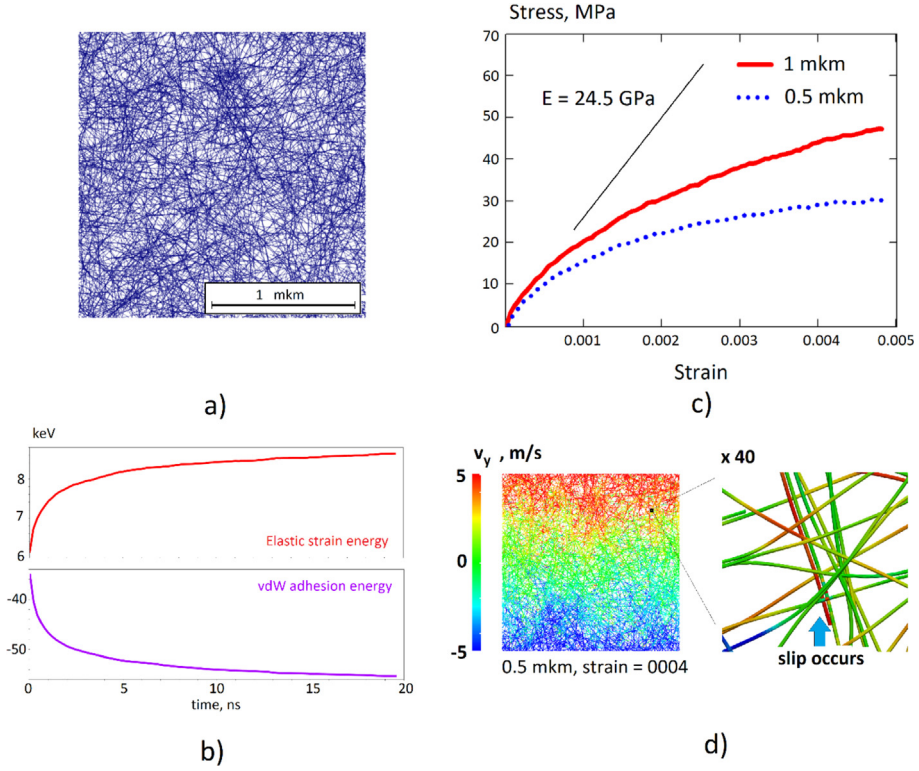

Fig. 5. (a) Specimen of a CNT film and schematics of biaxial mechanical test (b) Evolution of the potential energy terms during the relaxation of a 1 μm SWCNT film specimen. (c) Stress-strain curves observed in a biaxial test (d) Scalar field of the vertical velocity component, indicating the slipping of separate CNTs during plastic deformation. (A colour version of this figure can be viewed online.)

SWCNT film structure is characterized by a decrease in vdW adhesion energy due to the formation of bundles along with an increase in the elastic strain energy due to the bend of SWCNTs (Fig. 5b). At the second stage, the biaxial tension load was applied with a sufficiently low deformation rate to eliminate inertial effects, leaving a relatively small rate dependence associated with realistic energy dissipation during relative SWCNT slip. Biaxial tension was used to model the free-standing film bulge test described above.

Our numerical simulations have demonstrated results that are in good qualitative agreement with experimental data. The observed stress-strain curve (Fig. 5c) featured a linear elastic regime and an initial stage of deformation, followed by plastic flow. Yielding threshold in the model was approximately 0.1–0.2%. Biaxial modules of the film specimens were 26 GPa for 1 μm long SWCNTs and 22 GPa for 0.5 μm long SWCNTs. These parameters are in good agreement with those observed in experiment. However, the plastic yield stress was substantially lower. We attribute this difference to a greater SWCNT length and to a higher degree of bundling of SWCNTs in the film used in the experiment, since SWCNT bundling occurs not only on the filter during collection, as was simulated in the calculations, but also in the gas phase after their synthesis before the SWCNTs got collected on a filter.

Our simulation clearly demonstrated that plastic deformation of SWCNT films observed both in the experiment and in the simulation is conditioned by the relative slip of SWCNTs in the plane, as illustrated in Fig. 5d. The color in the left picture corresponds to the SWCNT velocity projection on the y-axis. One can see that closer to the edge SWCNTs have a greater speed in the direction of stretching, however, unlike bulk materials, the velocity field is non-uniformly distributed due to SWCNT straightening and slipping one past each other. It can be seen more clearly with a higher magnification (right picture) where neighboring SWCNTs have different velocities. Recent computational works [37,38] demonstrate that such a slip is not localized due to the stabilizing role of energy dissipation and does not lead to significant changes in the structure and properties of the SWCNTs, unless the strain reaches several tens of percent. At strains up to 10% such plastic flow does not lead to localized damage development.

5. Conclusions

We synthesized SWCNTs by an aerosol CVD method, fabricated freestanding thin films and examined their optical and mechanical properties. The method allows to produce specimens with lateral sizes of more than 10 cm and a thicknesses of from 10 to 100 nm which makes it very attractive for industrial applications. The soft X-ray and EUV transmittance spectra of a 40-nm film was measured using the synchrotron radiation. The measured transmittance at the operational wavelength of EUV lithography (13.5 nm) reached 88%, which meets the demands of various applications. The mechanical properties of the films were characterized by the bulge test. The stress-strain curve of the samples demonstrates the high ductility of the SWCNT films, which allows them to withstand high pressure loads. High performance numerical modeling using mesoscale technique was employed to understand the behavior of the film under strain at the microscale. We have shown that SWCNT slip is responsible for ductile behavior of the film preventing from brittle failure. The combination of high EUV transmittance and unique mechanical properties of the SWCNT films makes them extremely attractive for applications in EUV optics, and particularly, for fabrication of the protective pellicles for EUV photomask.

Acknowledgements

Mr. Andrei Starkov is acknowledged for helping to create 3D schematics of the experimental setup. The authors (V. Y. Y., Yu. G. G. and A.G.N.) acknowledge Russian Science Foundation (Project identifier: 17-19-01787) for the support of the experimental part of the research. I. O. acknowledges Russian Science Foundation (Project identifier: 17-73-10442) and Russian Foundation for Basic Research (Project identifier: 18-29-19198) for the support of numerical modeling parts of the work. The authors acknowledge the usage of Skoltech CDISE HPC cluster Zhores for obtaining the results presented in this paper.

References

[1] J.M. Schnorr, T.M. Swager, Emerging applications of carbon nanotubes, Chem. Mater. 23 (2011) 646–657, https://doi.org/10.1021/cm102406h.
[2] A.G. Nasibulin, A. Kaskela, K. Mustonen, A.S. Anisimov, V. Ruiz, S. Kivistö, S. Rackauskas, M.Y. Timmermans, M. Pudas, B. Aitchison, M. Kauppinen, D.P. Brown, O.G. Okhotnikov, E.I. Kauppinen, Multifunctional free-standing single-walled carbon nanotube films, ACS Nano 5 (2011) 3214–3221, https://doi.org/10.1021/nn200338r.
[3] V. Schroeder, S. Savagatrup, M. He, S. Lin, T.M. Swager, Carbon nanotube chemical sensors, Chem. Rev. 119 (2019) 599–663, https://doi.org/10.1021/acs.chemrev.8b00340.
[4] L. Yu, C. Shearer, J. Shapter, Recent development of carbon nanotube transparent conductive films, Chem. Rev. 116 (2016) 13413–13453, https://doi.org/10.1021/acs.chemrev.6b00179.
[5] Y. Cao, S. Cong, X. Cao, F. Wu, Q. Liu, MohR. Amer, C. Zhou, Review of electronics based on single-walled carbon nanotubes, in: Y. Li, S. Maruyama (Eds.), Single-Walled Carbon Nanotub. Prep. Prop. Appl, Springer International Publishing, Cham, 2019, pp. 189–224, https://doi.org/10.1007/978-3-030-12700-8_7.
[6] D. McCoul, W. Hu, M. Gao, V. Mehta, Q. Pei, Recent advances in stretchable and transparent electronic materials, Adv. Electron. Mater. 2 (2016) 1500407, https://doi.org/10.1002/aelm.201500407.
[7] C. Wagner, N. Harned, Lithography gets extreme, Nat. Photonics 4 (2010) 24.
[8] Igor Fomenkov, David Brandt, Alex Ershov, Schafgans Alexander, Yezheng Tao, Vaschenko Georgiy, Rokitski Slava, Kats Michael, Michael Vargas, Purvis Michael, Rafac Rob, La Fontaine Bruno, De Dea Silvia, LaForge Andrew, Jayson Stewart, Steven Chang, Graham Matthew, Riggs Daniel, Ted Taylor, Mathew Abraham, Daniel Brown, Light sources for high-volume manufacturing EUV lithography: technology, performance, and power scaling, Adv. Opt. Technol. 6 (2017) 173, https://doi.org/10.1515/aot-2017-0029.
[9] M.D. Seaberg, B. Zhang, D.F. Gardner, E.R. Shanblatt, M.M. Murnane, H.C. Kapteyn, D.E. Adams, Tabletop nanometer extreme ultraviolet imaging in an extended reflection mode using coherent Fresnel ptychography, Optica 1 (2014) 39–44, https://doi.org/10.1364/OPTICA.1.000039.
[10] W. Ackermann, G. Asova, V. Ayvazyan, A. Azima, N. Baboi, J. Bähr, V. Balandin, B. Beutner, A. Brandt, A. Bolzmann, R. Brinkmann, O.I. Brovko, M. Castellano, P. Castro, L. Catani, E. Chiadroni, S. Choroba, A. Cianchi, J.T. Costello, D. Cubaynes, J. Dardis, W. Decking, H. Delsim-Hashemi, A. Delserieys, G. Di Pirro, M. Dohlus, S. Düsterer, A. Eckhardt, H.T. Edwards, B. Faatz, J. Feldhaus, K. Flöttmann, J. Frisch, L. Fröhlich, T. Garvey, U. Gensch, Ch Gerth, M. Görler, N. Golubeva, H.-J. Grabosch, M. Grecki, O. Grimm, K. Hacker, U. Hahn, J.H. Han, K. Honkavaara, T. Hott, M. Hüning, Y. Ivanisenko, E. Jaeschke, W. Jalmuzna, T. Jezynski, R. Kammering, V. Katalev, K. Kavanagh, E.T. Kennedy, S. Khodyachykh, K. Klose, V. Kocharyan, M. Körfer, M. Kollewe, W. Koprek, S. Korepanov, D. Kostin, M. Krassilnikov, G. Kube, M. Kuhlmann, C.L.S. Lewis, L. Lilje, T. Limberg, D. Lipka, F. Löhl, H. Luna, M. Luong, M. Martins, M. Meyer, P. Michelato, V. Miltchev, W.D. Möller, L. Monaco, W.F.O. Müller, O. Napieralski, O. Napoly, P. Nicolosi, D. Nölle, T. Nuñez, A. Oppelt, C. Pagani, R. Paparella, N. Pchalek, J. Pedregosa-Gutierrez, B. Petersen, B. Petrosyan, G. Petrosyan, L. Petrosyan, J. Pflüger, E. Plönjes, L. Poletto, K. Pozniak, E. Prat, D. Proch, P. Pucyk, P. Radcliffe, H. Redlin, K. Rehlich, M. Richter, M. Roehrs, J. Roensch, R. Romaniuk, M. Ross, J. Rossbach, V. Rybnikov, M. Sachwitz, E.L. Saldin, W. Sandner, H. Schlarb, B. Schmidt, M. Schmitz, P. Schmüser, J.R. Schneider, E.A. Schneidmiller, S. Schnepp, S. Schreiber, M. Seidel, D. Sertore, A.V. Shabunov, C. Simon, S. Simrock, E. Sombrowski, A.A. Sorokin, P. Spanknebel, R. Spesyvtsev, L. Staykov, B. Steffen, F. Stephan, F. Stulle, H. Thom, K. Tiedtke, M. Tischer, S. Toleikis, R. Treusch, D. Trines, I. Tsakov, E. Vogel, T. Weiland, H. Weise, M. Wellhöfer, M. Wendt, I. Will, A. Winter, K. Wittenburg, W. Wurth, P. Yeates, M.V. Yurkov, I. Zagorodnov, K. Zapfe, Operation of a free-electron laser from the extreme ultraviolet to the water window, Nat. Photonics 1 (2007) 336.
[11] T. Shintake, H. Tanaka, T. Hara, T. Tanaka, K. Togawa, M. Yabashi, Y. Otake, Y. Asano, T. Bizen, T. Fukui, S. Goto, A. Higashiya, T. Hirono, N. Hosoda, T. Inagaki, S. Inoue, M. Ishii, Y. Kim, H. Kimura, M. Kitamura, T. Kobayashi, H. Maesaka, T. Masuda, S. Matsui, T. Matsushita, X. Maréchal, M. Nagasono, H. Ohashi, T. Ohata, T. Ohshima, K. Onoe, K. Shirasawa, T. Takagi, S. Takahashi, M. Takeuchi, K. Tamasaku, R. Tanaka, Y. Tanaka, T. Tanikawa, T. Togashi, S. Wu, A. Yamashita, K. Yanagida, C. Zhang, H. Kitamura, T. Ishikawa, A compact free-electron laser for generating coherent radiation in the extreme ultraviolet

region, Nat. Photonics 2 (2008) 555.
[12] E. Allaria, R. Appio, L. Badano, W.A. Barletta, S. Bassanese, S.G. Biedron, A. Borga, E. Busetto, D. Castronovo, P. Cinquegrana, S. Cleva, D. Cocco, M. Cornacchia, P. Craievich, I. Cudin, G. D'Auria, M. Dal Forno, M.B. Danailov, R. De Monte, G. De Ninno, P. Delgiusto, A. Demidovich, S. Di Mitri, B. Diviacco, A. Fabris, R. Fabris, W. Fawley, M. Ferianis, E. Ferrari, S. Ferry, L. Froehlich, P. Furlan, G. Gaio, F. Gelmetti, L. Giannessi, M. Giannini, R. Gobessi, R. Ivanov, E. Karantzoulis, M. Lonza, A. Lutman, B. Mahieu, M. Milloch, S.V. Milton, M. Musardo, I. Nikolov, S. Noe, F. Parmigiani, G. Penco, M. Petronio, L. Pivetta, M. Predonzani, F. Rossi, L. Rumiz, A. Salom, C. Scafuri, C. Serpico, P. Sigalotti, S. Spampinati, C. Spezzani, M. Svandrlik, C. Svetina, S. Tazzari, M. Trovo, R. Umer, A. Vascotto, M. Veronese, R. Visintini, M. Zaccaria, D. Zangrando, M. Zangrando, Highly coherent and stable pulses from the FERMI seeded free-electron laser in the extreme ultraviolet, Nat. Photonics 6 (2012) 699.
[13] G. Del Zanna, H.E. Mason, Solar UV and X-ray spectral diagnostics, Living Rev. Sol. Phys. 15 (2018) 5, https://doi.org/10.1007/s41116-018-0015-3.
[14] F.M. Quinn, D. Teehan, M. MacDonald, S. Downes, P. Bailey, Higher-order suppression in diffraction-grating monochromators using thin films, J. Synchrotron Radiat. 5 (1998) 783–785, https://doi.org/10.1107/S0909049597016440.
[15] E.B. Klyuenkov, A Ya Lopatin, V.I. Luchin, Nikolai N. Salashchenko, N.N. Tsybin, Freestanding film structures for laser plasma experiments, Quantum Electron. 43 (2013) 388.
[16] R. Sobierajski, R.A. Loch, R.W.E. van de Kruijs, E. Louis, G. von Blanckenhagen, E.M. Gullikson, F. Siewert, A. Wawro, F. Bijkerk, Mo/Si multilayer-coated amplitude-division beam splitters for XUV radiation sources, J. Synchrotron Radiat. 20 (2013) 249–257, https://doi.org/10.1107/S0909049512049990.
[17] S.P. Huber, V.V. Medvedev, J. Meyer-Ilse, E. Gullikson, B. Padavala, J.H. Edgar, J.M. Sturm, R.W.E. van de Kruijs, D. Prendergast, F. Bijkerk, Exploiting the P L2,3 absorption edge for optics: spectroscopic and structural characterization of cubic boron phosphide thin films, Opt. Mater. Express 6 (2016) 3946–3959, https://doi.org/10.1364/OME.6.003946.
[18] J.L.P. Barreaux, I.V. Kozhevnikov, M. Bayraktar, R.W.E. Van De Kruijs, H.M.J. Bastiaens, F. Bijkerk, K.-J. Boller, Narrowband and tunable anomalous transmission filters for spectral monitoring in the extreme ultraviolet wavelength region, Opt. Express 25 (2017) 1993–2008, https://doi.org/10.1364/OE.25.001993.
[19] N.I. Chkhalo, M.N. Drozdov, E.B. Kluenkov, S.V. Kuzin, A.Ya Lopatin, V.I. Luchin, N.N. Salashchenko, N.N. Tsybin, S.Yu Zuev, Thin film multilayer filters for solar EUV telescopes, Appl. Opt. 55 (2016) 4683–4690, https://doi.org/10.1364/AO.55.004683.
[20] Brouns Derk, Development and performance of EUV pellicles, Adv. Opt. Technol. 6 (2017) 221, https://doi.org/10.1515/aot-2017-0023.
[21] A. Moisala, A.G. Nasibulin, D.P. Brown, H. Jiang, L. Khriachtchev, E.I. Kauppinen, Single-walled carbon nanotube synthesis using ferrocene and iron pentacarbonyl in a laminar flow reactor, John Bridg. Symp. Shap. Future Chem. Eng. 61 (2006) 4393–4402, https://doi.org/10.1016/j.ces.2006.02.020.
[22] Y. Tian, A.G. Nasibulin, B. Aitchison, T. Nikitin, J.v. Pfaler, H. Jiang, Z. Zhu, L. Khriachtchev, D.P. Brown, E.I. Kauppinen, Controlled synthesis of single-walled carbon nanotubes in an aerosol reactor, J. Phys. Chem. C 115 (2011) 7309–7318, https://doi.org/10.1021/jp112291f.
[23] A. Kaskela, A.G. Nasibulin, M.Y. Timmermans, B. Aitchison, A. Papadimitratos, Y. Tian, Z. Zhu, H. Jiang, D.P. Brown, A. Zakhidov, E.I. Kauppinen, Aerosol-synthesized SWCNT networks with tunable conductivity and transparency by a dry transfer technique, Nano Lett. 10 (2010) 4349–4355, https://doi.org/10.1021/nl101680s.
[24] Image taken with free-standing SWCNT film, Produced by CANATU Oy (n.d.), https://canatu.com/) with the identical method discuss.
[25] F. Schäfers, P. Bischoff, F. Eggenstein, A. Erko, A. Gaupp, S. Künstner, M. Mast, J.-S. Schmidt, F. Senf, F. Siewert, A. Sokolov, Th Zeschke, The at-wavelength metrology facility for UV- and XUV-reflection and diffraction optics at BESSY-II, J. Synchrotron Radiat. 23 (2016) 67–77, https://doi.org/10.1107/S1600577515020615.
[26] A. Sokolov, P. Bischoff, F. Eggenstein, A. Erko, A. Gaupp, S. Künstner, M. Mast, J.-S. Schmidt, F. Senf, F. Siewert, Th Zeschke, F. Schäfers, At-wavelength metrology facility for soft X-ray reflection optics, Rev. Sci. Instrum. 87 (2016) 052005, https://doi.org/10.1063/1.4950731.
[27] A. Sokolov, M.G. Sertsu, A. Gaupp, M. Lüttecke, F. Schäfers, Efficient high-order suppression system for a metrology beamline, J. Synchrotron Radiat. 25 (2017) 100–107, https://doi.org/10.1107/S1600577517016800.
[28] S.-G. Kim, D.-W. Shin, T. Kim, S. Kim, J.H. Lee, C.G. Lee, C.-W. Yang, S. Lee, S.J. Cho, H.C. Jeon, M.J. Kim, B.-G. Kim, J.-B. Yoo, Large-scale freestanding nanometer-thick graphite pellicles for mass production of nanodevices beyond 10 nm, Nanoscale 7 (2015) 14608–14611, https://doi.org/10.1039/C5NR03079J.
[29] Dario L. Goldfarb, Fabrication of a full-size EUV pellicle based on silicon nitride, 96350A-9635–13, https://doi.org/10.1117/12.2196901, 2015.
[30] P.J. van Zwol, M. Nasalevich, W.P. Voorthuijzen, E. Kurganova, A. Notenboom, D. Vles, M. Peter, W. Symens, A.J.M. Giesbers, J.H. Klootwijk, R.W.E. van de Kruijs, W.J. van der Zande, Pellicle films supporting the ramp to HVM with EUV, 104510O-10451–9, https://doi.org/10.1117/12.2280560, 2017.
[31] G.F. Cardinale, R.W. Tustison, Fracture strength and biaxial modulus measurement of plasma silicon nitride films, Thin Solid Films 207 (1992) 126–130, https://doi.org/10.1016/0040-6090(92)90112-O.
[32] N.I. Chkhalo, S.V. Kuzin, A.Ya Lopatin, V.I. Luchin, N.N. Salashchenko, S.Yu Zuev, N.N. Tsybin, Improving the optical and mechanical characteristics of aluminum thin-film filters by adding thin cap layers, Thin Solid Films 653 (2018) 359–364, https://doi.org/10.1016/j.tsf.2018.03.051.
[33] I. Ostanin, R. Ballarini, D. Potyondy, T. Dumitrică, A distinct element method for large scale simulations of carbon nanotube assemblies, J. Mech. Phys. Solids 61 (2013) 762–782, https://doi.org/10.1016/j.jmps.2012.10.016.
[34] I. Ostanin, R. Ballarini, T. Dumitrică, Distinct element method modeling of carbon nanotube bundles with intertube sliding and dissipation, J. Appl. Mech. 81 (2014), https://doi.org/10.1115/1.4026484, 061004-061004–10.
[35] I. Ostanin, P. Zhilyaev, V. Petrov, T. Dumitrica, S. Eibl, U. Ruede, V. Kuzkin, Toward large scale modeling of carbon nanotube systems with the mesoscopic distinct element method, Lett. Mater. 8 (2018) 240–245.
[36] V.A. Kuzkin, I.E. Asonov, Vector-based model of elastic bonds for simulation of granular solids, Phys. Rev. E. 86 (2012) 051301, https://doi.org/10.1103/PhysRevE.86.051301.
[37] Y. Wang, G. Drozdov, E.K. Hobbie, T. Dumitrica, Excluded volume Approach for ultrathin carbon nanotube network stabilization: a mesoscopic distinct element method study, ACS Appl. Mater. Interfaces 9 (2017) 13611–13618, https://doi.org/10.1021/acsami.7b01434.
[38] Y. Wang, H. Xu, G. Drozdov, T. Dumitrică, Mesoscopic friction and network morphology control the mechanics and processing of carbon nanotube yarns, Carbon 139 (2018) 94–104, https://doi.org/10.1016/j.carbon.2018.06.043.